ACS OMEGA

http://pubs.acs.org/journal/acsodf

Article

Biomolecular Fishing: Design, Green Synthesis, and Performance of L-Leucine-Molecularly Imprinted Polymers

Ana I. Furtado, Raquel Viveiros, Vasco D. B. Bonifácio, André Melo, and Teresa Casimiro*

Cite This: *ACS Omega* 2023, 8, 9179−9186

Read Online

ACCESS | Metrics & More | Article Recommendations | Supporting Information

ABSTRACT: Biopurification is a challenging and growing market. Despite great efforts in the past years, current purification strategies still lack specificity, efficiency, and cost-effectiveness. The development of more sustainable functional materials and processes needs to address pressing environmental goals, efficiency, scale-up, and cost. Herein, L-leucine (LEU)-molecularly imprinted polymers (MIPs), LEU-MIPs, are presented as novel biomolecular fishing polymers for affinity sustainable biopurification. Rational design was performed using quantum mechanics calculations and molecular modeling for selecting the most appropriate monomers. LEU-MIPs were synthesized for the first time by two different green approaches, supercritical carbon dioxide ($scCO_2$) technology and mechanochemistry. A significant imprinting factor of 12 and a binding capacity of 27 mg LEU/g polymer were obtained for the LEU-MIP synthesized in $scCO_2$ using 2-vinylpyridine as a functional monomer, while the LEU-MIP using acrylamide as a functional monomer synthesized by mechanochemistry showed an imprinting factor of 1.4 and a binding capacity of 18 mg LEU/g polymer, both systems operating at a low binding concentration (0.5 mg LEU/mL) under physiological conditions. As expected, at a higher concentration (1.5 mg LEU/mL), the binding capacity was considerably increased. Both green technologies show high potential in obtaining ready-to-use, stable, and low-cost polymers with a molecular recognition ability for target biomolecules, being promising materials for biopurification processes.

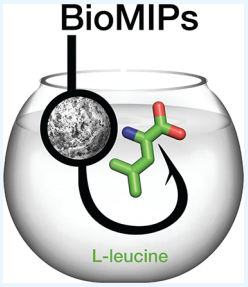

1. INTRODUCTION

Biopurification is increasing by 8.4% per year, and it is expected to reach 11.2 billion USD market by 2029.[1] However, there is still a lack of cost-effective strategies for biomolecules' purification, being the ones currently available expensive, inefficient, and/or with low specificity.[2] Nowadays, molecular imprinting is a viable synthetic approach to design robust molecular recognition materials, able to mimic natural systems, such as antibodies and other biological species with an affinity to specific biomolecules.[3] These advanced materials have applications in many areas such as biosensors and biopurification devices, being cost-effective and displaying low toxicity and accessible storage conditions.

Molecular imprinting polymerization involves the polymerization of functional monomers and crosslinking agents, using an adequate initiator and a porogenic solvent, in the presence of a template molecule. The obtained molecularly imprinted polymer (MIP) is a three-dimensional porous matrix possessing complementary cavities to the template in terms of size, conformation, and chemical functionality.[4]

The stability of the template−monomer complex is a key parameter for successful molecular recognition. Therefore, computational modeling has become a very important tool in MIP design for the rationalization of the molecular interactions intrinsic to the imprinting process, drastically reducing the experimental work.[5−7]

The most common porogenic solvents for the conventional synthesis of MIPs toward biomolecules (bio-MIPs) are acetonitrile and methanol, with a low water content to help the solubilization of biomolecules in the organic phase.[8−11] Unfortunately, water molecules can interfere with the interactions between the template and the functional monomer.[4] Also, in the production of conventional MIPs, large amounts of organic solvents are used, and their removal is not straightforward and can substantially increase the production costs. To circumvent these limitations, greener MIP synthesis using supercritical carbon dioxide ($scCO_2$) as a porogenic and template-extraction solvent has been successfully developed.[12−14] Likewise, mechanochemistry is a potential route for MIP green production since chemical transformations are induced by mechanical forces under solventless conditions.[15] Mechanochemistry has been quite explored in the synthesis of metal−organic frameworks (MOFs) and has shown to be a fast, simple, and efficient route for synthesis at solventless conditions, avoiding solubility issues.[16] Herein, we present the rational design and green synthesis of LEU-MIPs, MIPs with molecular recognition for L-leucine (LEU), an essential amino acid that plays an important role in biological systems (Figure 1). All polymers, LEU-MIPs and their corresponding nonimprinted polymers

Received: November 1, 2022
Accepted: January 20, 2023
Published: March 1, 2023

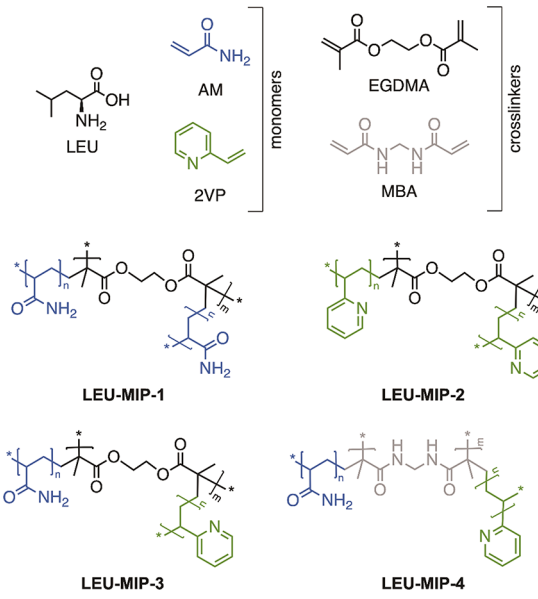

Figure 1. Chemical structures of L-leucine (LEU, template), functional monomers acrylamide (AM) and 2-vinylpyridine (2VP), crosslinkers ethylene glycol dimethacrylate (EGDMA) and *N*,*N*′-methylenebisacrylamide (MBA), and LEU-MIPs.

(NIPs) used as a control, were characterized, and their performance was evaluated in static binding experiments to assess the affinity to LEU.

2. EXPERIMENTAL SECTION

2.1. Materials. All commercial reagents and solvents were used as received without further purification. L-Leucine (LEU, 98%), 2-vinylpyridine (2VP, 97%), ethylene glycol dimethacrylate (EGDMA, 98%), *N*,*N*′-methylenebisacrylamide (MBA, 99%), sodium persulfate (≥98%), sodium chloride (NaCl, ≥99%), the acetonitrile solvent (ACN, ≥99.5%), and the methanol solvent (MeOH, ≥99.9%) were purchased from Sigma-Aldrich. Acrylamide (AM, >98%) was purchased from Fluka. The ethanol solvent (EtOH, ≥98% purity) was purchased from Honeywell-Fluka, the acetone solvent (99.5%) was purchased from PanReac AppliChem, and the ethyl acetate solvent (EtOAc, 99.5%) was provided by LabChem. 2,2′-Azobis(2,4-dimethylvaleronitrile) (V-65, 98%) was purchased from Wako Pure Chemical Industries. Phosphate-buffered saline (PBS) tablets were purchased from Sigma-Aldrich. Carbon dioxide was obtained from Air Liquide with a purity better than 99.998%. SnakeSkin dialysis membranes (3.5 kDa MWCO) were purchased from Thermo Fisher.

2.2. Quantum Mechanics Calculations. Nine functional monomers, commonly used in molecular imprinting polymerizations, 2-vinylpyridine (2VP), 4-vinylpyridine (4VP), acrylic acid (AA), acrylamide (AM), 2-acrylamido-2-methylpropane sulfonic acid (AMPS), itaconic acid (ITA), *N*-vinylpyrrolidone (NVP), styrene (STY), and 1-vinylimidazole (VIIM), were investigated as potential monomers for LEU-MIP syntheses. The initial fragments' (functional monomers and LEU) geometries were obtained from the literature,[6,17] and the template−monomer complexes' geometries were generated using a specific protocol described below. LEU is a very flexible amino acid, with eight main conformations.[17] Therefore, a multiconformational model for template−monomer binding was used in this work. For this purpose, the following procedure was adopted: the geometries of all the chemical species under study (initial fragments and template−monomer complexes) were fully optimized using the M06-2X/6-31+G(d) density functional theory (DFT) level. This quantum level has been proven to provide accurate results for similar systems,[6,18] once it can describe properly the dispersive interactions.[19] Analytic harmonic frequencies were calculated, to ensure that the optimized geometries correspond to genuine stationary states. The energetic stability of the LEU conformations was first analyzed. According to the results obtained, only the four most stable conformations were used in subsequent calculations. As the nine functional monomers were conformationally rigid, each of them was represented by a single unique optimized geometry. For each template−monomer complex, the monomer was first docked into the LEU conformational templates using the Autodock Vina program.[20,21] This procedure generated four conformational structures for each template−monomer complex. All the geometries obtained were then preoptimized at a PM6 or PDDG semiempirical level. Subsequently, two additional corrections were introduced in the electronic molar energy: (1) the description of the electronic density was improved, by performing M06-2X/6-311++G(3df,3pd) single-point calculations for all optimized geometries, and (2) counterpoise correction was applied for all complexes under study at the same quantum level to minimize the basis set superposition error (BSSE). From the two different combined quantum levels used in this work (geometry optimization and frequency calculation performed at a M06-2X/6-31+G(d) low quantum level and the electronic corrections carried out at a M06-2X/6-311++G(3df,3pd) high quantum level), the M06-2X/6-311++G(3df,3pd) level was chosen for using the counterpoise correction. All the previous calculations were performed using the Gaussian 09 program.[22]

The standard molar enthalpy, for each optimized structure, was obtained at a temperature of 25 °C and a pressure of 1 bar (standard conditions). For each template−monomer complex, the respective binding standard molar enthalpy ($\langle \Delta_{bind} H^{o} \rangle$) was calculated using eq 1.

$$\langle \Delta_{bind} H^{o} \rangle = \langle H_{m}^{o} \rangle_{complex} - \langle H_{m}^{o} \rangle_{LEU} - \langle H_{m}^{o} \rangle_{monomer} \quad (1)$$

where $\langle H_{m}^{o} \rangle_{complex}$ is the standard molar enthalpy for the template−monomer complex, $\langle H_{m}^{o} \rangle_{LEU}$ and $\langle H_{m}^{o} \rangle_{monomer}$ are the standard molar enthalpies for the initial fragments, LEU and monomer, respectively. $\langle H_{m}^{o} \rangle_{complex}$ and $\langle H_{m}^{o} \rangle_{LEU}$ were evaluated as a LEU-conformational average quantity following the Boltzmann population equation. All calculation results and equations used are included in the Supporting Information (see Tables S4 and S5).

A cluster analysis, using the binding standard molar enthalpy as a descriptor, was performed using StatSoft STATISTICA 64 software.[23] A complete linkage algorithm and a Euclidean distance were used in this analysis (see Figure S1, Supporting Information).

Further studies were performed for different temperatures and pressures of the system using the thermodynamic equations (see Figure S2, Supporting Information).

2.3. LEU-MIP Synthesis. The MIPswere produced using two different monomers, 2-vinylpyridine (2VP) and acrylamide (AM), and two different crosslinkers, ethylene glycol dimethacrylate (EGDMA) and *N*,*N*′-methylenebisacrylamide

https://doi.org/10.1021/acsomega.2c05714
ACS Omega 2023, 8, 9179−9186

(MBA) (Figure 1), with a molar ratio template:monomer:-crosslinker (T:M:C) of 1:50:100.

For the LEU-MIP synthesis in $scCO_2$, a reported protocol was followed.[13] $ScCO_2$-assisted polymerization was carried out in a 33 mL high-pressure cell, using a template:monomer:-crosslinker (T:M:C) molar ratio of 1:50:100 and 2 wt % V-65 (total weight % of the monomer and the crosslinker) as the initiator. LEU was previously dissolved in 0.5 mL of EtOAc and kept under stirring for 4 h. All reagents were placed in the high-pressure cell, with a magnetic stirring bar, and immersed in a thermostatic water bath at 45 °C. CO_2 was loaded up to 200 bar using a Knauer K-1900 liquid pump. After 24 h of reaction, a homogeneous crosslinked polymer was obtained. At the end of the reaction, the polymer was slowly washed with fresh CO_2 for 1 h to remove unreacted starting materials. The NIP was synthesized following the same procedure, but the EtOAc cosolvent was added without the template (LEU).

For the LEU-MIP mechanosynthesis, mechanochemical polymerization was performed in a PM100 planetary ball mill (Retsch) using a zirconium oxide reactor containing 200 zirconium oxide balls of 5 mm diameter. The reaction occurred for 6 h, at 500 rpm, with rotation inversion cycles of 30 min (2.5 min pause between inversion cycles). The T:M:C molar ratio (1:50:100) was the same as that used in the $scCO_2$-assisted polymerization. Sodium persulfate (10 wt %) (total weight % of the monomer and the crosslinker) was used as the initiator, and NaCl (2 times the total weight) was added as a porogenic agent. At the end of the reaction, 10 mL of distilled water was added to the reactor, and the mixture was ground for 2 min at 500 rpm to help polymer collection from the reactor and balls. The mixture was then collected using a pipette, filtrated under vacuum, and further washed with water and methanol to remove unreacted starting materials. The recovered polymer was dried under a vacuum system. The NIP was synthesized following the same procedure but without template (LEU) addition.

2.4. $ScCO_2$-Assisted LEU Desorption. LEU desorption was performed to obtain LEU-MIPs with empty binding sites, ready for molecular fishing (LEU rebinding). LEU desorption was performed using a well-established $scCO_2$ continuous extraction process.[13] For that, a tubular column was loaded and compacted with the synthesized polymer and coupled to a 33 mL stainless steel high-pressure cell with 3 mL of EtOAc, and the system was pressurized with CO_2 up to 200 bar. Both high-pressure cells were immersed in a thermostated water bath at 40 °C. CO_2 was bubbled through the cell containing the cosolvent (bottom to top), and the mixture CO_2−EtOAc was passed through the tubular reactor in the continuous mode for 3 h.

2.5. High-Pressure Ion Chromatography (HPIC) Quantification. LEU ion chromatographic analysis was carried out using a Dionex ICS3000 equipment with an electrochemical detector for pulsed amperometry detection (PAD) and an Aminopac PA10 250 × 4 mm column with a precolumn of 50 × 4 mm as the stationary phase, at 30 °C.[24] The mobile phase contained a NaOH gradient solution at a constant flow of 0.8 mL/min. The injection volume of the LEU samples was 10 μL. A plot of the electrochemical signal (nC) as a function of the LEU concentration was performed to obtain the calibration curve. The standard solutions were obtained by dilution of the most concentrated solution used for calibration. All samples were diluted with a factor of 10×.

2.6. Scanning Electron Microscopy. The morphology of the polymers was assessed by SEM using a Hitachi S-2400 instrument with an accelerating voltage set to 15 kV. Samples were mounted on aluminum stubs using carbon tape and were gold-coated. A 5000× magnification was used.

2.7. Average Particle Size and Particle Size Distribution. Particle size distribution, as well as average particle size diameters of polymers, was determined using a Morphologi G3 equipment from Malvern. A typical analysis was performed by dispersing the sample using the following conditions: a sample volume of 13 mm^3, SDU settings (injection pressure: 4 bar, injection time: 40 ms, and setting time: 120 s), and an optic selection of 20×. The analyses were performed in triplicate from three different dispersions with at least 30 000 particles counted.

2.8. Specific Surface and Pore Diameter. Polymers' specific surface area and pore diameter were determined by N_2 adsorption according to the BET method. An accelerated surface area and porosimetry system (ASAP 2010 Micromeritics) was used under N_2 flow.

2.9. Fourier Transform Infrared Spectroscopy. FTIR spectra of the polymers were recorded in a PerkinElmer Two spectrometer, with 16 scans and a resolution of 1 cm^{-1} in the range of 4000 to 400 cm^{-1}.

2.10. Static Binding Assays. The binding capacity of the produced polymers was evaluated on PBS buffer solutions using two LEU concentrations (0.5 and 1.5 mg/mL). In the static binding assay, a 20 mg polymer sample was placed into Snakeskin dialysis membrane bags and introduced in a 25 mL template solution, for 24 h, under stirring at 100 rpm (IKA KS 4000 I Control shaker). After this period, the polymer binding 1 mL of the solution was filtered and analyzed by HPIC. The binding capacity Q (mg LEU/mg LEU-MIP) was calculated using eq 2:

$$Q = \frac{(C_0 - C)V}{W} \tag{2}$$

where C_0 and C are the template concentrations (mg LEU/mL) in the solutions measured initially and after sorption, respectively, V (mL) is the volume of the solution, and W (mg) is the sample polymer weight. The imprinting factor (IF) was calculated using eq 3:

$$\mathrm{IF} = \frac{Q_{\mathrm{MIP}}}{Q_{\mathrm{NIP}}} \tag{3}$$

where Q_{MIP} is the binding capacity of the molecularly imprinted polymer and Q_{NIP} is the binding capacity of the nonimprinted polymer. The IF is a simple estimation to describe the imprinting effect. The tests were performed in triplicated assays of each polymer, and all static binding data are presented in the Supporting Information (see Table S9 and Table S10).

3. RESULTS AND DISCUSSION

3.1. Computational Studies: Monomer Selection. In noncovalent imprinting, a stronger interaction between the monomer and the template leads to a more effective imprinting effect.[25] Mimicking prepolymerization steps by computational methods, noncovalent combination interactions, mostly hydrogen bonds between the monomer and the template were observed, resulting in different conformations of the template−monomer complex. This computational strategy could provide

https://doi.org/10.1021/acsomega.2c05714
ACS Omega 2023, 8, 9179−9186

information about the most suitable monomer for MIP preparation. Table 1 shows the binding energies, $\langle \Delta_{bind}H^{o} \rangle$, of LEU−monomer complexes, as well as the number of hydrogen bonds (n) and the electric dipole moment (EDM) of the lowest energy conformation complex obtained, data divided by the cluster.

Table 1. Binding Energies ($\langle \Delta_{bind}H^{o} \rangle$) of LEU−Monomer Complexes Obtained at the Counterpoise M06-2X/6-311++G(3df,3pd) Level, Monomer Nature, the Electric Dipole Moment (EDM), and the Number of Hydrogen Bonds (n) for Each Lowest Energy Conformation Complex, Divided by the Cluster[a]

cluster	LEU−monomer complex	monomer nature	$\langle \Delta_{bind}H^{o} \rangle$ (kJ mol^{-1})	EDM (D)	n
1	LEU-AM	neutral	−57.86	3.7468	2
2	LEU-AMPS	basic	−45.63	4.3864	1
	LEU-NVP	basic	−42.69	2.1226	1
	LEU-ITA	acidic	−41.26	7.0456	2
3	LEU-AA	acidic	−33.26	1.6571	1
	LEU-4VP	basic	−26.03	4.8179	1
	LEU-STY	neutral	−23.27	4.6525	0
	LEU-VIIM	basic	−22.61	4.5374	0
	LEU-2VP	basic	−21.25	2.6587	0

[a]1 being a more suitable complex to 3 being a less suitable complex.

The data suggest that AM is the most suitable monomer to get a more stable LEU−monomer complex with the highest binding energy. On the other hand, 2VP was found to be the monomer less favored to form stable LEU−monomer complexes. According to the data, the nature of the monomer (neutral, acidic, or basic) is not directly related to the formation of more stable LEU−monomer complexes; however, the number of hydrogen bond interactions might play an important role, resulting in a higher number of hydrogen bond interactions with more acidic monomers.

One of the factors that seem to be important for T:M complex stabilization is the monomer configuration and the presence of substituents and their position in the molecule. This is well-illustrated in the case of 2VP and 4VP monomers, which are both basic monomers and similar in size but where the nitrogen position in the pyridine ring was found to influence the complex stabilization. Notwithstanding, the binding energy values calculated for vinylpyridine monomers are quite similar, being both in the same cluster. Considering the quantum mechanics calculations, AM and 2VP monomers were chosen for the synthesis of LEU-MIPs, with AM as the best functional monomer and 2VP as the worst functional monomer. The optimized geometries of LEU-AM and LEU-2VP complexes are presented in Figure 2.

Since the polymerization in $scCO_2$ needs to be carried out at 45 °C and 200 bar, thermodynamic calculations were also performed at different temperatures (25, 45, and 65 °C) and pressures (1, 100, 200, and 300 bar) (see Figure S2, Supporting Information). As expected, the binding energies ($\langle \Delta_{bind}H \rangle$) of both LEU-AM and LEU-2VP complexes are influenced by temperature, showing a LEU−monomer complex destabilization with increasing temperature. Pressure variation had no impact in the $\langle \Delta_{bind}H \rangle$ of both systems. Altogether, these findings showed that the polymerization temperature must be the lowest possible (*i.e.*, a temperature above and close to the critical temperature of CO_2 while allowing a homogeneous polymerization).

3.2. LEU-MIP and NIP Synthesis and Characterization.

Since LEU has a low solubility in $scCO_2$,[26] a cosolvent is required to increase its solubility and thus achieve an initial homogeneous phase. Solubility tests in $scCO_2$, under the same conditions as polymerization with different cosolvents (MeOH, EtOH, EtOAc, ACN, and acetone) were performed, revealing EtOAc as the best organic cosolvent for the LEU-MIP reaction system. This drawback is usually overcome through derivatization methods such as amino acid esterization,[27] while herein, it is overcome by adding a small amount of one of the greenest organic solvents commercially available. Dry, fluffy free-flowing, white powders were obtained in $scCO_2$ up to 40% yield (see Table S6, Supporting Information), as reported for MIPs synthesized in $scCO_2$ for different classes of molecules.[28,29] The low yield could be explained by the lower polymerization temperature (45 °C), which is below the optimum half-life decomposition temperature of the V-65 initiator (*ca.* 50 °C). Three LEU-MIPs: **LEU-MIP$_{sc}$-1** (AM-EGDMA), **LEU-MIP$_{sc}$-2** (2VP-EGDMA), and **LEU-MIP$_{sc}$-3** (AM-2VP-EGDMA) and their corresponding NIPs: **NIP$_{sc}$-1** (AM-EGDMA), **NIP$_{sc}$-2** (2VP-EGDMA), and **NIP$_{sc}$-3** (AM-2VP-EGDMA) were successfully synthesized using this methodology. An initial homogeneous phase before polymerization was not possible using the T:M:C molar ratio of 1:50:100 and MBA as a crosslinker due to the low solubility of MBA in $scCO_2$; thus, this polymer was not further characterized or tested.

A major advantage of mechanochemistry is the elimination of solubility issues since the reactions are performed under solventless conditions. LEU-MIPs and NIPs synthesized by mechanochemistry were obtained as dry, fine powders with yields up to 80% (see Table S6, Supporting Information). MIP

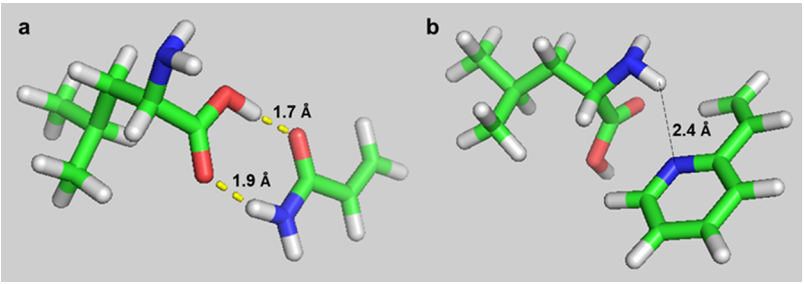

Figure 2. Optimized geometry of LEU−monomer complexes: (a) LEU-AM complex, showing two very strong well-oriented hydrogen bond interactions and distance measurements, and (b) LEU-2VP complex showing the close distance between the hydrogen from the LEU amine group and the nitrogen from 2VP. Carbon atoms are green, nitrogen atoms are blue, oxygen atoms are red, and hydrogen atoms are light gray.

https://doi.org/10.1021/acsomega.2c05714
ACS Omega 2023, 8, 9179−9186

mechanosynthesis is still not reported in the literature, and to the best of our knowledge, this is also the first report of MIP synthesis using a biomolecule (LEU) as a template, both using an $scCO_2$-assisted polymerization and mechanochemistry. Four LEU-MIPs: **LEU-MIP$_m$-1** (AM-EGDMA), **LEU-MIP$_m$-2** (2VP-EGDMA), **LEU-MIP$_m$-3** (AM-2VP-EGDMA), and **LEU-MIP$_m$-4** (AM-2VP-MBA) and the corresponding NIPs: **NIP$_m$-1** (AM-EGDMA), **NIP$_m$-2** (2VP-EGDMA), **NIP$_m$-3** (AM-2VP-EGDMA), and **NIP$_m$-4** (AM-2VP-MBA) were synthesized using this methodology.

SEM, Morphologi G3, and ASAP were used to characterize the polymers' morphology. SEM images are shown in Figure 3. As it can be seen, polymers are formed by particle agglomerates.

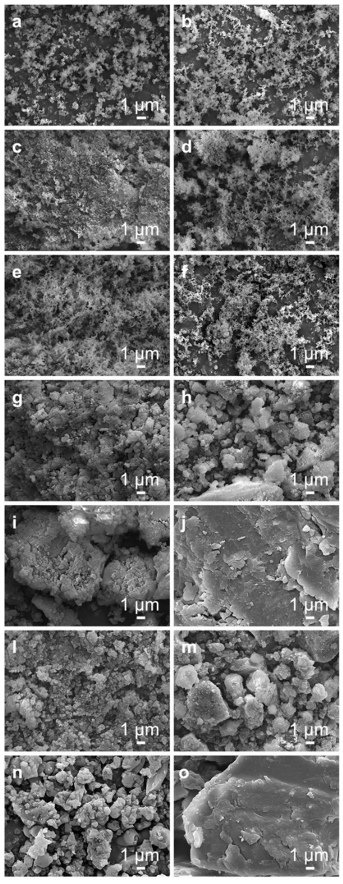

Figure 3. SEM images at 5000× magnification of the polymers synthesized using $scCO_2$: (a) **LEU-MIP$_{sc}$-1**, (b) **NIP$_{sc}$-1**, (c) **LEU-MIP$_{sc}$-2**, (d) **NIP$_{sc}$-2**, (e) **LEU-MIP$_{sc}$-3**, and (f) **NIP$_{sc}$-3** and synthesized by mechanochemistry: (g) **LEU-MIP$_m$-1**, (h) **NIP$_m$-1**, (i) **LEU-MIP$_m$-2**, (j) **NIP$_m$-2**, (l) **LEU-MIP$_m$-3**, (m) **NIP$_m$-3**, (n) **LEU-MIP$_m$-4**, and (o) **NIP$_m$-4**.

The particle size distribution and the corresponding images are presented in the Supporting Information (Figures S4 and S5), as well as the average particle size diameter, the specific surface area, the pore volume, and pore size (Table S7). In general, the average particle size diameter obtained was between 1 and 3 μm, with MIPs showing higher values than the NIPs, which could be related to the presence of LEU in the polymerization step. Polymers presented type-II and type-IV isotherms, which are indicative of macroporous and/or mesoporous structures, except **NIP$_m$-2** and **NIP$_m$-4** (see Figure S6, Supporting Information).

Comparing the SEM images, a higher agglomeration is observed in the polymers obtained by mechanochemistry, which is consistent with the higher average particle size diameter and particle size distribution determined. Polymers containing 2VP (**LEU-MIP$_{sc}$-2**, **NIP$_{sc}$-2**, **LEU-MIP$_m$-2**, and **NIP$_m$-2**) present a denser structure and smaller particle agglomerates than AM-containing polymers (**LEU-MIP$_{sc}$-1**, **NIP$_{sc}$-1**, **LEU-MIP$_m$-1**, and **NIP$_m$-1**), which also explain the lower average particle diameter trend. The observed morphological differences may be attributed to the chosen synthetic methods, much different in terms of the interactions involved in the particle's growth (solvent *vs.* solventless conditions). In addition, comparing the MIPs with the corresponding NIPs in both methodologies, it is clear that the reaction components slightly affect the particle size, which is in agreement with reports of MIPs produced using $scCO_2$ and in conventional media.[28,30,31]

Regarding porosimetry, the ASAP isotherm linear plots presented some hysteresis that is characteristic of mesoporous materials.[32] The gas uptake, at a low P/P_0, by polymers obtained using $scCO_2$ also indicates the existence of micropores, not observed in those obtained by mechanochemical polymerization. According to the surface area, pore volume, and average pore size diameter data, a significant difference was obtained using both methodologies. Polymers obtained by mechanosynthesis display much lower specific surface areas (<10 m^2/g) and pore volumes (<0.17 cm^3/g), possessing predominantly macropores and a smaller fraction of mesopores. The use of salts, like NaCl, as porogenic agents in mechanochemical reactions, has been reported (*e.g.*, preparation of porous MOFs) in a process known as salt-assisted grinding (SAG).[33] Through this method, micro-, meso-, and even macroporous polymeric materials could be obtained. However, as already mentioned, the produced polymers displayed a lower porosity (18−46 nm range) if compared with other reported systems.[34−36]

FTIR data (Figure S3 and Table S8, Supporting Information) show the presence of the characteristic monomer and crosslinker vibration bands, being clear, as expected after polymerization, the disappearance of the vibration band from the vinylic groups (~1650 cm^{-1}).

3.3. Binding Performance. The binding capacity of the produced LEU-MIPs was also evaluated. Figure 4 shows the binding data for LEU-MIPs synthesized in $scCO_2$ (**LEU-MIP$_{sc}$-1**, **LEU-MIP$_{sc}$-2**, and **LEU-MIP$_{sc}$-3**), by mechanochemistry (**LEU-MIP$_m$-1**, **LEU-MIP$_m$-2**, **LEU-MIP$_m$-3**, and **LEU-MIP$_m$-4**), and their counterpart NIPs, using two LEU different concentrations (0.5 and 1.5 mg/mL) at pH 7.4. The imprinting factors were also determined (Table 2).

LEU-MIPs$_m$ prepared by mechanochemistry show binding performances that are in line with quantum mechanics calculations (Table 1) since a higher binding capacity was obtained by the **LEU-MIP$_{m-1}$** that used AM as a functional monomer (Figure 4c). On the other hand, LEU-MIPs$_{sc}$ prepared in $scCO_2$ do not follow the computational prediction, obtaining a higher binding performance for the LEU-MIP$_{sc-2}$ that used 2VP as a functional monomer (Figure 4a). This opposite trend between the theoretical and practical results might be related to the $scCO_2$ effect as a solvent during the imprinting process since our quantum calculations were performed without the presence of a solvent.

https://doi.org/10.1021/acsomega.2c05714
ACS Omega 2023, 8, 9179−9186

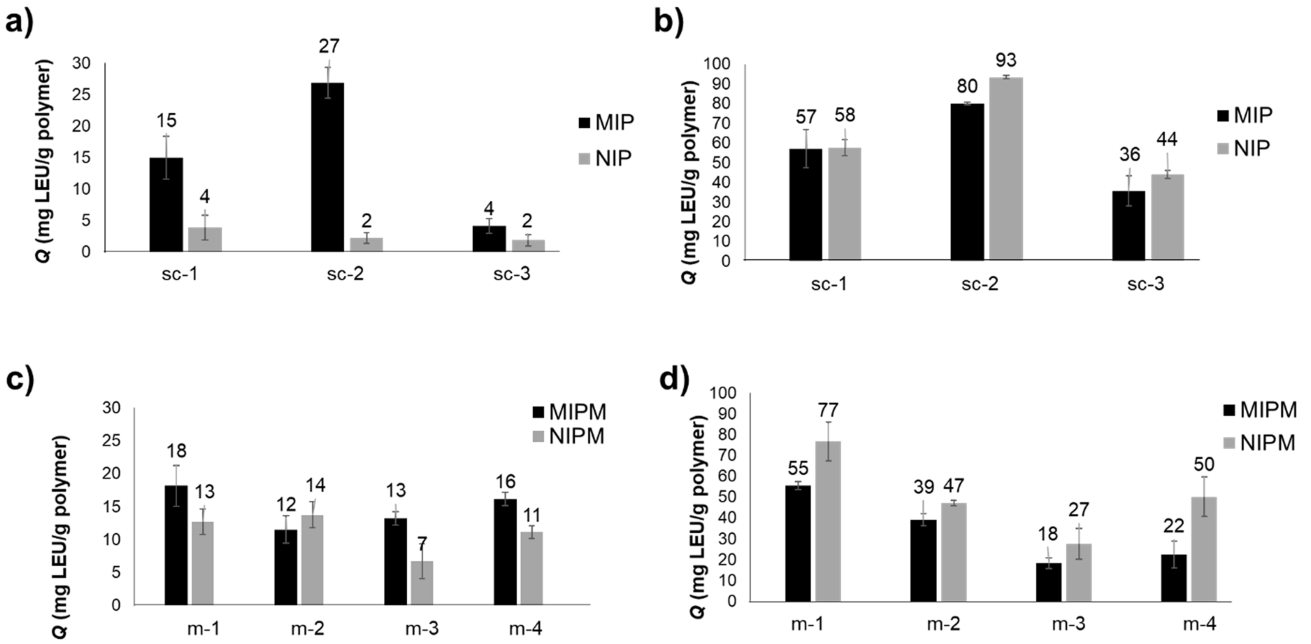

Figure 4. Binding assays of LEU-MIPs obtained using $scCO_2$ ($_{sc}$-**1**, $_{sc}$-**2**, and $_{sc}$-**3**) at (a) 0.5 and (b) 1.5 mg LEU/mL and for polymers obtained by mechanochemistry ($_{m}$-**1**, $_{m}$-**2**, $_{m}$-**3**, and $_{m}$-**4**) at (c) 0.5 and (d) 1.5 mg LEU/mL.

Table 2. Imprinting Factors for LEU-MIPs

	IF	
polymer	0.5 mg LEU/mL	1.5 mg LEU/mL
LEU-MIP$_{sc}$-1	3.86	0.99
LEU-MIP$_{sc}$-2	12.05	0.86
LEU-MIP$_{sc}$-3	2.16	0.81
LEU-MIP$_{m}$-1	1.43	0.72
LEU-MIP$_{m}$-2	0.84	0.83
LEU-MIP$_{m}$-3	1.98	0.66
LEU-MIP$_{m}$-4	1.45	0.45

Viveiros et al. introduced CO_2 for the first time as a solvent in the computational approach for MIP synthesis, to understand its effect on molecular modeling of the monomer−template.[5] According to this molecular dynamics study using SYBYL software, CO_2 could have a significant effect on template−monomer interactions.[5] In our study, in order to assess the contribution of CO_2 to the template−monomer complex, the electric dipole moment (EDM) of each complex was calculated (Table 1) and compared with the EDM of CO_2 at the polymerization conditions. The calculated EDM of the complex LEU-AM (3.7468 D) was higher than that for the complex LEU-2VP (2.6587 D), being this latter closer to the EDM of $scCO_2$ (1.4821 D at 200 bar and 45 °C[37]). The template−monomer complexes with an EDM lower and closer to the solvent EDM could reflect a more stable conformation of its template−monomer complex and consequently envisage a better molecular recognition performance.[38,39] Despite being a different approach compared to Viveiros et al.'s study, the dielectric constants can serve as an indicator to describe the observed binding results.

Regarding the practical results, the best performance was achieved for **LEU-MIP$_{sc}$-2**, presenting a very significant imprinting factor of 12 and a binding capacity of 27 mg LEU/g polymer. **LEU-MIP$_{m}$-1**, with an imprinting factor of 1.4 and a binding capacity of 18 mg LEU/g polymer, was also found to be an interesting system.

The polymers synthesized with the combination of the two monomers (2VP and AM) exhibited a lower binding capacity than the polymers synthesized with only one monomer. A possible explanation could be attributed to monomers competing for LEU, resulting in polymer conformations with nonspecific recognition sites, also reported in the literature in computational simulations of mimicking the prepolymerization imprinting process to proteins.[40] The crosslinking effect was evaluated for LEU-MIPs obtained by mechanochemistry. A higher binding capacity was observed for **LEU-MIP$_{m}$-4** (16 mg LEU/g polymer, MBA) in comparison with **LEU-MIP$_{m}$-3** (13 LEU/g polymer, EGDMA), but a lower imprinting factor was obtained, indicating that MBA promotes a greater number of nonspecific bindings. Rational MIP design studies suggest that the best crosslinkers should be inert toward the template, displaying lower interactions, thus improving specificity and selectivity.[41]

As expected, for a higher LEU concentration (1.5 *vs.* 0.5 mg/mL), the binding capacities increased, a trend also observed for NIPs, but low imprinting factors were also observed in this case (<1). Some studies on biomolecule recognition by MIPs reported the use of similar concentrations (0.5−1.5 mg/mL),[42,43] although the use of lower concentrations is much more common. Despite the higher binding capacities reported on these systems (up to 400 mg biomolecule/g MIP *vs.* 80 mg LEU/g MIP in this work), lower IFs are found (*ca.* 2), highlighting the importance of $scCO_2$ as a green alternative for the production of materials with high IFs.[14,28]

4. CONCLUSIONS

The most suitable monomer for LEU, AM, was selected using quantum mechanics calculations. Based on *in silico* performance, LEU-molecularly imprinted polymers were successfully synthesized using two green strategies, $scCO_2$-assisted polymerization and mechanosynthesis. LEU-MIP$_{sc}$ using 2VP as the monomer and EGDMA as a crosslinker was found to be the most selective, presenting a maximum IF of 12. In contrast,

https://doi.org/10.1021/acsomega.2c05714
ACS Omega 2023, 8, 9179−9186

the best performance for LEU-MIPs$_m$ was obtained using AM as the monomer and EGDMA as a crosslinker, with a maximum IF of 2. The imprinting effect was evidently higher at a low LEU concentration (0.5 mg LEU/mL), with a maximum binding capacity of 27 mg LEU/g polymer. A binding capacity increase was observed for a higher concentration (1.5 mg LEU/mL), achieving a maximum binding capacity of 93 mg LEU/g polymer.

Overall, LEU-MIPs are envisaged as potential advanced materials for demanding biopurification late-stage downstream processes (*e.g.*, chromatography columns), where affinity and efficiency and scale-up possibilities are critical assets.

■ ASSOCIATED CONTENT

Supporting Information

The Supporting Information is available free of charge at https://pubs.acs.org/doi/10.1021/acsomega.2c05714.

Quantum mechanics calculations and MIP and NIP characterization data (polymerization yield, physical properties, ASAP isotherms, and FTIR spectra) (PDF)

■ AUTHOR INFORMATION

Corresponding Author

Teresa Casimiro − *Chemistry Department, NOVA School of Science & Technology, LAQV-REQUIMTE, NOVA University of Lisbon, Caparica 2829-516, Portugal;* orcid.org/0000-0001-9405-6221; Email: teresa.casimiro@fct.unl.pt

Authors

Ana I. Furtado − *Chemistry Department, NOVA School of Science & Technology, LAQV-REQUIMTE, NOVA University of Lisbon, Caparica 2829-516, Portugal; iBB-Institute for Bioengineering and Biosciences and i4HB-Institute for Health and Bioeconomy, Instituto Superior Técnico, University of Lisbon, Lisboa 1049-001, Portugal;* orcid.org/0000-0003-3502-5147

Raquel Viveiros − *Chemistry Department, NOVA School of Science & Technology, LAQV-REQUIMTE, NOVA University of Lisbon, Caparica 2829-516, Portugal;* orcid.org/0000-0002-0449-2343

Vasco D. B. Bonifácio − *iBB-Institute for Bioengineering and Biosciences and i4HB-Institute for Health and Bioeconomy, Instituto Superior Técnico, University of Lisbon, Lisboa 1049-001, Portugal; Bioengineering Department, Instituto Superior Técnico, University of Lisbon, Lisboa 1049-001, Portugal;* orcid.org/0000-0003-2349-8473

André Melo − *Departamento de Química e Bioquímica, Faculdade de Ciências, LAQV-REQUIMTE, Universidade do Porto, Porto 4169-007, Portugal;* orcid.org/0000-0001-6455-7834

Complete contact information is available at: https://pubs.acs.org/10.1021/acsomega.2c05714

Author Contributions

The manuscript was written with the contributions of all authors. All authors have approved the final version of the manuscript.

Notes

The authors declare no competing financial interest.

■ ACKNOWLEDGMENTS

The authors would like to acknowledge financial support from Fundação para a Ciência e a Tecnologia, Ministério da Ciência, Tecnologia e Ensino Superior (FCT/MCTES), Portugal, through projects PTDC/EQU-EQU/32473/2017, PTDC/MEC-ONC/29327/2017, and PTDC/QUI-QIN/30649/2017 (REALM). A.I.F. acknowledges her PhD grant (SFRH/BD/150696/2020) in the aim of the International Year of the Periodic Table—a protocol established between the Portuguese Chemical Society (SPQ) and the Portuguese Foundation for Science and Technology (FCT/MCTES). R.V. would like to acknowledge Individual Scientific Employment Stimulus (CEEC-IND), reference 2020.00377.CEECIND from the FCT/MCTES, Portugal. The Associate Laboratory Research Unit for Green Chemistry−Clean Technologies and Processes−LAQV-REQUIMTE is financed by national funds from FCT/MCTES (UIDB/50006/2020, UIDP/50006/2020, and UID/QUI/50006/2020) and cofinanced by the ERDF under the PT2020 Partnership Agreement (POCI-01-0145-FEDER−007265).

■ REFERENCES

(1) *Protein Purification and Isolation Market − Global Industry Trends and Forecast to 2029* https://www.databridgemarketresearch.com/reports/global-protein-purification-isolation-market (accessed May 03, 2022).

(2) Khanal, O.; Lenhoff, A. M. Developments and Opportunities in Continuous Biopharmaceutical Manufacturing. *mAbs* **2021**, *13*, 1−13.

(3) Hoshino, Y.; Kodama, T.; Okahata, Y.; Shea, K. J. Peptide Imprinted Polymer Nanoparticles: A Plastic Antibody. *J. Am. Chem. Soc.* **2008**, *130*, 15242−15243.

(4) Vasapollo, G.; Sole, R. D.; Mergola, L.; Lazzoi, M. R.; Scardino, A.; Scorrano, S.; Mele, G. Molecularly Imprinted Polymers: Present and Future Prospective. *Int. J. Mol. Sci.* **2011**, *12*, 5908−5945.

(5) Viveiros, R.; Karim, K.; Piletsky, S. A.; Heggie, W.; Casimiro, T. Development of a Molecularly Imprinted Polymer for a Pharmaceutical Impurity in Supercritical CO_2: Rational Design Using Computational Approach. *J. Cleaner Prod.* **2017**, *168*, 1025−1031.

(6) Rebelo, P.; Pacheco, J. G.; Voroshylova, I. V.; Melo, A.; Cordeiro, M. N. D. S.; Delerue-Matos, C. Rational Development of Molecular Imprinted Carbon Paste Electrode for Furazolidone Detection: Theoretical and Experimental Approach. *Sens. Actuators, B* **2021**, *329*, 129112−129123.

(7) Nicholls, I. A.; Golker, K.; Olsson, G. D.; Suriyanarayanan, S.; Wiklander, J. G. The Use of Computational Methods for the Development of Molecularly Imprinted Polymers. *Polymer* **2021**, *13*, 1−40.

(8) Özcan, A. A.; Say, R.; Denizli, A.; Ersöz, A. L-Histidine Imprinted Synthetic Receptor for Biochromatography Applications. *Anal. Chem.* **2006**, *78*, 7253−7258.

(9) Hart, B. R.; Shea, K. J. Synthetic Peptide Receptors: Molecularly Imprinted Polymers for the Recognition of Peptides Using Peptide-Metal Interactions. *J. Am. Chem. Soc.* **2001**, *123*, 2072−2073.

(10) Scorrano, S.; Mergola, L.; del Sole, R.; Vasapollo, G. Synthesis of Molecularly Imprinted Polymers for Amino Acid Derivates by Using Different Functional Monomers. *Int. J. Mol. Sci.* **2011**, *12*, 1735−1743.

(11) Leonhardt, A. Enzyme-Mimicking Polymers Exhibiting Specific Substrate Binding and Catalytic Functions. *React. Funct. Polym.* **1987**, *6*, 285−290.

(12) Viveiros, R.; Rebocho, S.; Casimiro, T. Green Strategies for Molecularly Imprinted Polymer Development. *Polymer* **2018**, *10*, 1−27.

(13) Furtado, A. I.; Viveiros, R.; Casimiro, T. MIP Synthesis and Processing Using Supercritical Fluids. *Mol. Imprinted Polym.* **2021**, *2359*, 19−42.

(14) Viveiros, R.; Bonifácio, V. D. B.; Heggie, W.; Casimiro, T. Green Development of Polymeric Dummy Artificial Receptors with Affinity for Amide-Based Pharmaceutical Impurities. *ACS Sustainable Chem. Eng.* **2019**, *7*, 15445−15451.
(15) Do, J. L.; Friščic, T. Mechanochemistry: A Force of Synthesis. *ACS Cent. Sci.* **2017**, *3*, 13−19.
(16) Howard, J. L.; Cao, Q.; Browne, D. L. Mechanochemistry as an Emerging Tool for Molecular Synthesis: What Can It Offer? *Chem. Sci.* **2018**, *9*, 3080−3094.
(17) Dokmaisrijan, S.; Lee, V. S.; Nimmanpipug, P. The Gas Phase Conformers and Vibrational Spectra of Valine, Leucine and Isoleucine: An Ab Initio Study. *J. Mol. Struct.* **2010**, *953*, 28−38.
(18) Rebelo, P.; Pacheco, J. G.; Cordeiro, M. N. D. S.; Melo, A.; Delerue-Matos, C. Azithromycin Electrochemical Detection Using a Molecularly Imprinted Polymer Prepared on a Disposable Screen-Printed Electrode. *Anal. Methods* **2020**, *12*, 1486−1494.
(19) Suryana, S.; Mutakin; Rosandi, Y.; Hasanah, A. N. An Update on Molecularly Imprinted Polymer Design through a Computational Approach to Produce Molecular Recognition Material with Enhanced Analytical Performance. *Molecules* **2021**, *26*, 1891.
(20) Eberhardt, J.; Santos-Martins, D.; Tillack, A. F.; Forli, S. AutoDock Vina 1.2.0: New Docking Methods, Expanded Force Field, and Python Bindings. *J. Chem. Info. Model.* **2021**, *61*, 3891−3898.
(21) Trott, O.; Olson, A. J. AutoDock Vina: Improving the Speed and Accuracy of Docking with a New Scoring Function, Efficient Optimization and Multithreading. *J. Comput. Chem.* **2010**, *31*, 455−461.
(22) Frisch, M. J.; Trucks, G. W.; Schlegel, H. B.; Scuseria, G. E.; Robb, M. A.; Cheeseman, J. R.; Scalmani, G.; Barone, V.; Mennucci, B.; Petersson, G. A.; Nakatsuji, H.; Caricato, M.; Li, X.; Hratchian, H. P.; Izmaylov, A. F.; Bloino, J.; Zheng, G.; Sonnenberg, J. L.; Hada, M.; Ehara, M.; Toyota, K.; Fukuda, R.; Hasegawa, J.; Ishida, M.; Nakijima, T.; Honda, Y.; Kitao, O.; Nakai, H.; Vreven, T.; Montgomery, J. A., Jr.; Peralta, J. E.; Ogliaro, F.; Bearpark, M.; Heyd, J. J.; Brothers, E.; Kudin, K. N.; Staroverov, V. N.; Keith, T.; Kobayashi, R.; Normand, J.; Raghavachari, K.; Rendell, A.; Burant, J. C.; Iyengar, S. S.; Tomasi, J.; Cossi, M.; Rega, N.; Millam, J. M.; Klene, M.; Knox, J. E.; Cross, J. B.; Bakken, V.; Adamo, C.; Jaramillo, J.; Gomperts, R.; Stratmann, R. E.; Yazyev, O.; Austin, A. J.; Cammi, R.; Pomelli, C.; Ochterski, J. W.; Martin, R. L.; Morokuma, K.; Zakrzewski, V. G.; Voth, G. A.; Salvador, P.; Dannenberg, J. J.; Dapprich, S.; Daniels, A. D.; Farkas, O.; Foresman, J. B.; Ortiz, J. V.; Cioslowski, J.; Fox, D. J. *Gaussian 09*; Gaussian Inc.: Wallingford CT. 2013.
(23) *STATISTICA*; StatSoft, Inc. 2004.
(24) *Technical Note S0 Determination of the Amino Acid Content of Peptides by AAA-Direct*; ThermoFisher Scientific, AppsLab Library, 2015.
(25) Liu, Z.; Xu, Z.; Wang, D.; Yang, Y.; Duan, Y.; Ma, L.; Lin, T.; Liu, H. A Review on Molecularly Imprinted Polymers Preparation by Computational Simulation-Aided Methods. *Polymer* **2021**, *13*, 2657−2675.
(26) Ribeira Santos, I.; Thies, C.; Richard, J.; Meurlay, D.; Gajan, V.; Vandevelde, V.; Benoit, J.-P. Supercritical Fluid-Based Coating Technology. 2: Solubility Considerations. *J. Microencaps.* **2010**, *20*, 97−109.
(27) Baskal, S.; Bollenbach, A.; Tsikas, D. Two-Step Derivatization of Amino Acids for Stable-Isotope Dilution GC−MS Analysis: Long-Term Stability of Methyl Ester-Pentafluoropropionic Derivatives in Toluene Extracts. *Molecules* **2021**, *26*, 1726−1736.
(28) Viveiros, R.; Inês, M.; Heggie, W.; Casimiro, T. Green Approach on the Development of *Lock-and-Key* Polymers for API Purification. *Chem. Eng. J.* **2017**, *308*, 229−239.
(29) Marcelo, G.; Ferreira, I. C.; Viveiros, R.; Casimiro, T. Development of Itaconic Acid-Based Molecular Imprinted Polymers Using Supercritical Fluid Technology for PH-Triggered Drug Delivery. *Int. J. Pharm.* **2018**, *542*, 125−131.
(30) Rebocho, S.; Cordas, C. M.; Viveiros, R.; Casimiro, T. Development of a Ferrocenyl-Based MIP in Supercritical Carbon Dioxide: Towards an Electrochemical Sensor for Bisphenol A. *J. Supercrit. Fluids* **2018**, *135*, 98−104.
(31) Xizhi, S.; Aibo, W.; Guorun, Q.; Rongxiu, L.; Dabing, Z. Development and Characterisation of Molecularly Imprinted Polymers Based on Methacrylic Acid for Selective Recognition of Drugs. *Biomaterials* **2007**, *28*, 3741−3749.
(32) Anovitz, L. M.; Cole, D. R. Characterization and Analysis of Porosity and Pore Structures. *Rev. Mineral. Geochem.* **2015**, *80*, 61−164.
(33) Tao, C.-A.; Wang, J.-F. Synthesis of Metal Organic Frameworks by Ball-Milling. *Crystals* **2021**, *11*, 15−35.
(34) Steenhaut, T.; Grégoire, N.; Barozzino-Consiglio, G.; Filinchuk, Y.; Hermans, S. Mechanochemical Defect Engineering of HKUST-1 and Impact of the Resulting Defects on Carbon Dioxide Sorption and Catalytic Cyclopropanation. *RSC Adv.* **2020**, *10*, 19822−19831.
(35) Yang, J.; Feng, X.; Lu, G.; Li, Y.; Mao, C.; Wen, Z.; Yuan, W. NaCl as a Solid Solvent to Assist the Mechanochemical Synthesis and Post-Synthesis of Hierarchical Porous MOFs with High I2 Vapour Uptake. *Dalton Trans.* **2018**, *47*, 5065−5071.
(36) Le Bolay, N.; Santran, V.; Dechambre, G.; Combes, C.; Drouet, C.; Lamure, A.; Rey, C. Production, by Co-Grinding in a Media Mill, of Porous Biodegradable Polylactic Acid−Apatite Composite Materials for Bone Tissue Engineering. *Powder Technol.* **2009**, *190*, 89−94.
(37) Moriyoshi, T.; Kita, T.; Uosaki, Y. Static Relative Permittivity of Carbon Dioxide and Nitrous Oxide up to 30 MPa. *Ber. Bunsenges. Phys. Chem.* **1993**, *97*, 589−596.
(38) Rosengren, A. M.; Golker, K.; Karlsson, J. G.; Nicholls, I. A. Dielectric Constants Are Not Enough: Principal Component Analysis of the Influence of Solvent Properties on Molecularly Imprinted Polymer-Ligand Rebinding. *Biosens. Bioelectron.* **2009**, *25*, 553−557.
(39) Tarannum, N.; Singh, M. Selective Recognition and Detection of L-Aspartic Acid by Molecularly Imprinted Polymer in Aqueous Solution. *J. Anal. Chem.* **2011**, *02*, 909−918.
(40) Kryscio, D. R.; Shi, Y.; Ren, P.; Peppas, N. A. Molecular Docking Simulations for Macromolecularly Imprinted Polymers. *Ind. Eng. Chem. Res.* **2011**, *50*, 13877.
(41) Muhammad, T.; Nur, Z.; Piletska, E. V.; Yimit, O.; Piletsky, S. A. Rational Design of Molecularly Imprinted Polymer: The Choice of Cross-Linker. *Analyst* **2012**, *137*, 2623−2628.
(42) Xu, R.; Tian, J.; Guan, Y.; Zhang, Y. Peptide-Cross-Linked Protein-Imprinted Polymers: Easy Template Removal and Excellent Imprinting Effect. *CCS Chem.* **2019**, *1*, 544−552.
(43) Chen, Z.; Hua, Z.; Xu, L.; Huang, Y.; Zhao, M.; Li, Y. Protein-Responsive Imprinted Polymers with Specific Shrinking and Rebinding. *J. Mol. Recognit.* **2008**, *21*, 71−77.

https://doi.org/10.1021/acsomega.2c05714
ACS Omega 2023, 8, 9179−9186